Three-dimensional time-dependent modeling of high-power fiber amplifiers

G. Ronald Hadley[†], Roger L. Farrow[‡], and Arlee V. Smith[†]

[†]P. O. Box 5800, Sandia National Laboratories, Albuquerque, NM 87185
[‡]P. O. Box 969, Sandia National Laboratories, Livermore, CA 94550

Abstract

The design and optimization of high-power fiber amplifiers requires a simulation tool capable of including a wide range of effects simultaneously, including mode distortion and loss due to bending, spatially-dependent saturable gain, guiding from arbitrary index of refraction profiles and self-focusing. In addition, the nonlinear effects are power dependent and thus will distort the pulse shape. We have constructed a numerical model to address these issues and serve as a platform for data analysis and system optimization.

I. Introduction

The optimization of high-power fiber amplifiers requires the exploration of a very large multidimensional parameter space. Performing such a search in the laboratory would be prohibitively time-consuming and costly, and thus the need is clear for a comprehensive numerical model to handle this task. Although such a model need not include every effect present, it should include those which limit output power and energy, or influence the pulse width or output spectrum. Thus, it is important that space and time-dependent saturable gain be treated. And since gain saturation is sensitive to mode area, it follows that arbitrary fiber shapes and index profiles, and the mode distortion due to fiber bending and self-focusing should also be included. At present, there is, to the best of the authors' knowledge, no existing simulation tool that includes these physical effects in a single model. Existing models do not include the transverse beam profile and are therefore forced to employ effective mode areas to predict saturated output powers. These mode areas are difficult to estimate, and the predicted results are highly sensitive to this parameter (see section IIIA below), with the result that the mode area becomes almost a fitting parameter. In contrast, the model reported here is an *a priori* prediction with no fitting parameters employed at all.

To address the above modeling requirements, we have constructed a time-dependent three-dimensional model (denoted CFPULS for Coiled Fiber PUlsed Laser Simulator) of the propagation of a light pulse through an optically-pumped fiber amplifier. Because the fibers in use are a few meters or less in length we have neglected group velocity dispersion, since it typically requires kilometers of propagation to affect changes in pulse shape. As a result, the pulse may be divided into "slices" in the time domain, with each slice independent of the others except for changes in gain due to saturation. This approximation allows each time slice to be modeled using beam propagation according to an equation that will be developed in some detail in section II. This in turn affords orders of magnitude decreases in computation time and storage compared with a direct 3D time-

dependent solution of Maxwell's Equations. The aforementioned beam propagation is accomplished in our model using previously developed finite difference software[1] appropriate for bent fibers of arbitrary shape and index profile. This beam propagation module is then applied to each time slice and is accompanied by a saturable, two-level gain model using an initial inversion that may depend arbitrarily on all three spatial coordinates.

Details of our model and assumptions inherent in the derivation of equations are discussed in section II. In section III we compare the results of our 3D model with our previously-developed 1D time-dependent model and also with experimental data. The 1D comparisons aptly illustrate the shortcomings of modeling that does not include finite beam size effects. The good agreement with experiment serves to underscore the validity and usefulness of the 3D model.

II. Derivation of Equations

a. Optical field

Due to the small index contrast present between the fiber core and cladding, we keep only a single component of the optical field, say H. Starting with the time-dependent Maxwell Equations with a current source $J = \sigma E$ to include gain, standard manipulations yield the transient equation

$$\nabla^2 H - \mu_0 \varepsilon_0 \varepsilon \frac{\partial^2 H}{\partial t^2} - \mu_0 \sigma \frac{\partial H}{\partial t} = 0 \qquad (1)$$

where ε is the relative permittivity. For pure harmonic fields proportional to $e^{-i\omega t}$ this becomes

$$\nabla^2 H + k^2 \frac{\varepsilon}{\overline{\varepsilon}} H + i\mu_0 \sigma \omega H = 0 \qquad (2)$$

where we have introduced the vacuum wavevector $k_0 = \dfrac{\omega_0}{c}$, $\overline{\varepsilon}$ is a constant to be defined later, and $k^2 = k_0^2 \overline{\varepsilon}$. At this point, H is considered to be function of $\mathbf{x}, \omega$, where $\mathbf{x}$ stands for the spatial vector (x, y, z). In order to produce a transient equation, we sum over a range of frequencies centered at ω_0 with amplitude function $A(\omega - \omega_0)$, and let both k and σ depend on ω. We use the expansions

$$k^2 = k_0^2 \overline{\varepsilon} + (\omega - \omega_0) \frac{\partial k^2}{\partial \omega}\bigg|_{\omega_0} + \frac{1}{2}(\omega - \omega_0)^2 \frac{\partial^2 k^2}{\partial \omega^2}\bigg|_{\omega_0}$$

$$\sigma = \sigma_0 + (\omega - \omega_0) \frac{\partial \sigma}{\partial \omega}\bigg|_{\omega_0} + \frac{1}{2}(\omega - \omega_0)^2 \frac{\partial^2 \sigma}{\partial \omega^2}\bigg|_{\omega_0} \qquad (3)$$

and the fact that under the integral sign $(\omega - \omega_0) \rightarrow i\dfrac{\partial}{\partial t}$. For gain bandwidths of order 100 nm and pulse widths of nanoseconds,

$$(\omega - \omega_0)\frac{\partial \sigma}{\partial \omega} \approx \frac{i\sigma}{c\Delta k\tau} \approx 5\times 10^{-6} i\sigma_0$$

and we neglect all derivatives of σ. With the following definition of the new time-dependent field

$$\mathrm{H}(\mathbf{x},t) = \int A(\omega - \omega_0)H(\mathbf{x},\omega)e^{-i(\omega-\omega_0)t}d\omega \tag{4}$$

we may multiply (2) by A and integrate to get

$$\nabla^2 \mathrm{H} + k_0^2(\varepsilon + i\varepsilon_i)\mathrm{H} + 2ik\frac{\varepsilon}{\overline{\varepsilon}}\frac{\partial k}{\partial\omega}\Big|_{\omega_0}\frac{\partial \mathrm{H}}{\partial t} - \frac{\varepsilon}{2\overline{\varepsilon}}\frac{\partial^2 k}{\partial\omega^2}\Big|_{\omega_0}\frac{\partial^2 \mathrm{H}}{\partial t^2} - \mu_0\sigma_0\frac{\partial \mathrm{H}}{\partial t} = 0 \tag{5}$$

where we have defined the imaginary part of the dielectric constant by $k_0^2\varepsilon_i = \mu_0\omega_0\sigma_0$. We next identify some of the derivatives in (5) with well-known quantities:

$$\frac{\partial k}{\partial\omega} = \frac{1}{v_g}$$

$$\frac{\partial^2 k^2}{\partial\omega^2} = 2\left(\frac{\partial k}{\partial\omega}\right)^2 + 2k\frac{\partial^2 k}{\partial\omega^2} = \frac{2}{v_g^2} + 2k\beta_2 \tag{6}$$

with v_g the group velocity and β_2 the group velocity dispersion. We neglect the latter quantity for fibers of a few meters' length, since changes in pulse width due to GVD normally happen on a length scale of kilometers. We insert the relations (6) into (5) and also remove the fast phase variation along the propagation direction in the usual way (leading to the definition of $\overline{\varepsilon}$ referred to earlier). This results in

$$\nabla_\perp^2 \mathrm{H} + \frac{\partial^2 \mathrm{H}}{\partial z^2} + 2ik\frac{\partial \mathrm{H}}{\partial z} + k_0^2(\varepsilon - \frac{i\overline{n}g}{k_0} - \overline{\varepsilon})\mathrm{H} + \left(\frac{2ik\varepsilon}{v_g\overline{\varepsilon}} + \frac{g}{v_g}\right)\frac{\partial \mathrm{H}}{\partial t} - \frac{\varepsilon}{v_g^2\overline{\varepsilon}}\frac{\partial^2 \mathrm{H}}{\partial t^2} = 0 \tag{7}$$

where we have defined the power gain $g \equiv -\dfrac{k_0\varepsilon_i}{\overline{n}}$ ($\overline{n} = \sqrt{\overline{\varepsilon}}$). We next transform into a moving coordinate system centered on the pulse via

$$z' = z$$

$$t' = t - \frac{z}{v_g} \tag{8}$$

and recognize that the small index contrast between fiber core and cladding allows the approximation $\varepsilon \approx \overline{\varepsilon}$. In addition,

$$\frac{2}{v_g}\frac{\partial^2 \mathrm{H}}{\partial z'\partial t'} \approx \frac{g}{v_g}\frac{\partial \mathrm{H}}{\partial t'} \tag{9}$$

leading to the final equation

$$\frac{\partial \mathrm{H}}{\partial z'} = \frac{i}{2k}\left[\nabla_\perp^2 \mathrm{H} + \frac{\partial^2 \mathrm{H}}{\partial z'^2} + k_0^2(\varepsilon - \frac{i\overline{n}g}{k_0} - \overline{\varepsilon})\mathrm{H}\right] \tag{10}$$

It is apparent that Eq. (10) has the form of a time-independent beam propagation equation, except that (1) H is a function of both z' and t'; thus each "time slice" of the optical pulse propagates independently of all other slices, and (2) the properties functions ε and g can be time dependent, so that, for example, gain depletion from the

pulse leading edge may result in both a shape distortion and temporal broadening of the pulse.

In order to accommodate bending, Eq. (10) is expressed in a cylindrical coordinate system and finite difference equations derived on a triangular grid, as described previously[1,2]. This procedure allows a natural treatment of the effects of fiber bending, including mode distortion and loss without the necessity of incorporating *ad hoc* index ramping. Gain and nonlinear index changes were separated from the propagation matrix and incorporated into a single diagonal matrix using a decades-old approach[3] sometimes referred to as the "gain-sheet" approximation. This technique alleviates the standard requirement of re-inverting the propagation matrix whenever the gain or index profile changes, resulting in a tremendous savings in computer runtime. Self-focusing effects are included by incrementing the index of refraction according to the local power density via the standard relation

$$n = n_0(\mathbf{x}) + n_2 \left| \mathrm{H}(\mathbf{x},t) \right|^2 \tag{11}$$

Some comments are appropriate here concerning the numerical effort required to perform a system simulation of reasonable length using this model. For a transverse grid of 320 x 80 a single propagation step required 0.13 seconds on a modern workstation. For a temporal profile modeled with 30 time slices, this translates to 4 sec per propagation step for the whole pulse. Using propagation step sizes typical of other beam propagation simulations (~ 1 μm) we see that a 1m simulation would take over a month, clearly an unacceptable result. Consequently an investigation was undertaken concerning the use of much larger propagation steps. The conclusion of this work was that large propagation steps (as much as 0.8 mm, limited only by the energy gain per step) were allowable provided the spatial profile was constant, i.e. the beam was an eigenmode. However, if the bend radius was changing or self-focusing effects were present, large steps led to nonphysical transfer of energy to lossy modes, and consequently nonphysical energy loss. In these cases the understanding is that if several modes are present, the physical beat length for any two modes (particularly if one is lossy) must be adequately resolved by the propagation step in order to avoid nonphysical coupling between modes. This implies that the modeling of transition regions will require more time, or perhaps need to be addressed using a different modeling tool.

 b. Gain medium
We model the gain medium as a generalized two-level system with different degeneracies in the upper and lower states so that the absorption and emission cross sections are not equal. Then at any fixed position in space the occupation densities change according to

$$\frac{\partial n_u(\mathbf{x},t)}{\partial t} = (\sigma_a n_l(\mathbf{x},t) - \sigma_e n_u(\mathbf{x},t)) \frac{\left| \mathrm{H}(\mathbf{x},t) \right|^2}{\hbar \omega}$$

$$\frac{\partial n_l(\mathbf{x},t)}{\partial t} = (\sigma_e n_u(\mathbf{x},t) - \sigma_a n_l(\mathbf{x},t)) \frac{\left| \mathrm{H}(\mathbf{x},t) \right|^2}{\hbar \omega} \tag{12}$$

where $\sigma_{e,a}$ are the emission and absorption cross sections, respectively, and we have assumed that all other processes affecting state populations such as pumping, non-radiative relaxation and spontaneous emission are slow compared with the pulse width. Thus the picture we are proposing is that all processes other than stimulated emission act to establish an initial population inversion (in general a function of all spatial variables) from which the amplified pulse extracts a fraction of the stored energy as it passes by. This initial inversion is computed externally and read in as an input file prior to execution.

If we define the gain coefficient as $g \equiv \sigma_e n_u - \sigma_a n_l$ then simple manipulation of the equations in (12) yields

$$\frac{\partial g}{\partial t} = -(\sigma_e + \sigma_a)g\frac{|\mathrm{H}(\mathbf{x},t)|^2}{\hbar\omega} \tag{13}$$

which integrates immediately to give

$$g(\mathbf{x},t) = g_0(\mathbf{x})e^{-\frac{\sigma_e+\sigma_a}{\hbar\omega}\int_{-\infty}^{t}|\mathrm{H}(\mathbf{x},t')|^2 dt'} \tag{14}$$

where $g_0(\mathbf{x})$ is the initial gain distribution prior to the arrival of the pulse. Equation (14) thus provides a prediction of the gain as a function of both space and time, including saturation effects. A printout of the exponential in (14) gives a direct measure of the degree of saturation that, if averaged over the fiber cross section, is a useful number for the experimenter.

III. Benchmark Results

a. Comparison with 1D simulation

Here we compare computed results between the 3D code and a 1D code (ZT) employing similar physics except for the absence of lateral spatial effects. Thus the latter predicts output intensities and energy densities rather than power and beam energy, and consequently requires an effective beam area in order to compare with predictions by the 3D code. For both simulations we employed an initial inversion profile computed using a simple deposition model for an end-pumped fiber. For the 3D code the inversion profile was assumed to be constant across the fiber core and zero outside the core. A seed pulse with 1 ns duration and 0.1 mJ of energy was launched into one end of the fiber and propagated for 1m. For the 3D code the initial mode was the eigenmode of a bent fiber with a constant bend radius of 9 mm and a core diameter of 30 μm. For the 1D code a variety of intensities were input that were scaled to the same initial 0.1 mJ by multiplying by an effective beam area. No attempt was made to include a bend loss in the 1D simulations because it was small compared with the gain present in the fiber. Although self-focusing effects were included in the 3D simulation, they were found to be negligible for the powers encountered.
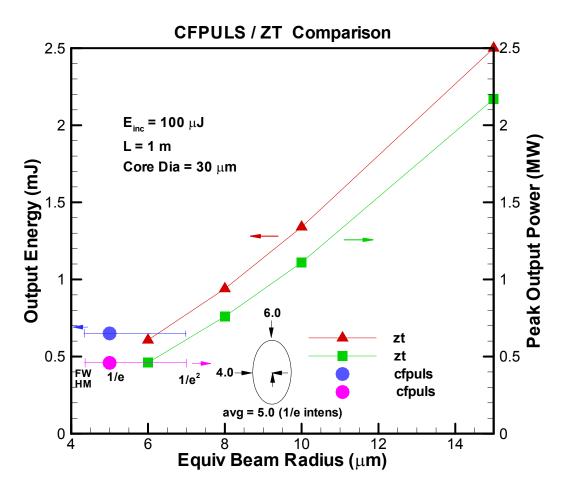
Fig. 1. Predicted peak power and output beam energy for a sample amplified pulse propagating over 1 m of end-pumped fiber.

The predicted peak output powers and beam energies for both simulations are shown in Fig. 1, and the output pulse widths in Fig. 2. Fig. 1 shows the 3D code predictions as data points with the approximate elliptical beam shape shown in the inset. The 1D predictions are shown as curves plotted vs. effective beam radius, and in general display a wide variety of numbers that are quite sensitive to the value of this parameter. Based on the beam shape shown and a 1/e radius of 5 μm, the 3D values were plotted at this value of beam radius for comparison with the 1D results. However, if FWHM values or $1/e^2$ values were used instead, the points could be plotted anywhere inside the error bars shown. Thus two conclusions are possible from these results: (1) Use of the 1D code for system output predictions is problematic unless some consistent formula for assigning a beam radius is available. In this case, a value about halfway between the 1/e and $1/e^2$ values seems to work well. (2) The two codes give consistent values of output energy and peak output power for a given value of beam radius, providing some confidence in the accuracy of the 3D code.

Predictions of output pulse width are shown in Fig. 2 for both codes. As can be seen, both predict pulse broadening due to strong gain saturation by the pulse leading edge. Agreement between the two is good for the same value of beam radius that resulted in good agreement for peak power and energy in Fig. 1. In this case, however, the predicted pulse width by the 3D code is somewhat uncertain (see error bars in the figure) due to the coarseness of the time grid used to define the pulse shape, whereas the 1D code could use extremely fine time slices without undue effort, and offered a more detailed prediction of broadening.
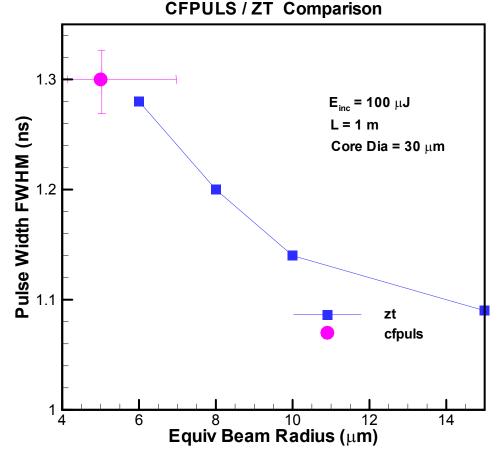

Fig. 2. Output pulse width predicted by both models

b. Comparison with experiment

In this comparison, the 3D code was employed to predict the output energy extracted from a 2-m-long Liekki 30/250PM fiber with a core diameter of 27.9 μm. The fiber was end-pumped from the output end with a diode laser running CW whose output power was varied from zero to 21.5 W, and injected with a 1.12 ns 1.6 μJ seed pulse at 1.064 μm wavelength at a repetition rate of 35.7 kHz. The amplified output was sufficient to saturate the fiber gain, but not high enough to see significant effects from self-focusing

or other nonlinear mechanisms such as stimulated Raman scattering (SRS), so the primary test was of the gain-saturation features of the model. The initial inversion was provided by the Liekki Application Designer (LAD) software, which simulates the diode pump beam propagation through the fiber, including effects from ASE and absorption using a measured diode laser emission spectrum and known frequency-dependent cross-sections. Output from the LAD code for each pump power as a function of distance along the fiber was read in as input for the simulation code, assuming uniform gain across the fiber core and zero outside the core.

In reality, a typical fiber amplifier (and the present experiment) consists of a large section of coiled fiber with a coil radius carefully chosen to offer just enough bend loss to discriminate against all high order modes, but small enough to affect the fundamental mode only marginally. This transition should ideally be taken into account, since the effective mode area changes significantly between the bent and straight fundamental eigenmode. However, for the following simulations, the bent eigenmode of the fiber (bend radius of 2.45 cm, index contrast of 0.00169) was used as the seed input, and transitions from bent to straight at the fiber ends were ignored, in order to use large propagation steps and thus reduce runtimes. A check of this approximation for the largest pump power showed a 7.5% increase in output when the straight 15-cm-long output section was modeled using a larger mode (with a resulting reduced gain saturation from 60% to 49%). However, the inclusion of insertion losses resulting from the transition from bent to straight, which was not included, would be expected to reduce this enhancement somewhat.
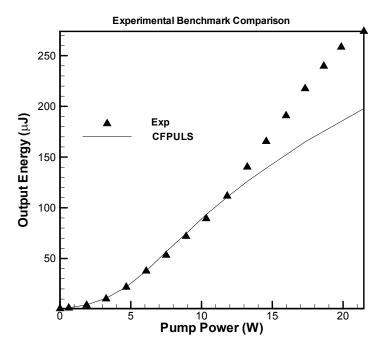

Fig. 3. Comparison between predicted and measured output powers for a 2m-long end-pumped fiber described in detail in the text. The discrepancy at high pump powers is at

present thought to result from a change in experimental conditions, but is not well understood.

The results from this simulation are shown in Fig. 3. Note that the model is entirely predictive, with no adjustable parameters. As can be seen, the predictions are quite accurate up to a pump power of 11.81W, after which the measured energies turn upward compared with the simulation results. We believe that this discrepancy reflects inaccuracies in the computed initial inversion profile at the higher pump powers. Establishment of the initial inversion profile represents a complicated process in which excitation by the CW pump light is balanced by the high-repetition-rate amplified seed pulse. Although loss of inversion due to amplified stimulated emission (ASE) is included in the inversion calculations, this mechanism is difficult to model, and is expected to be more influential at the higher pump powers. Nonetheless, the model predictions are still within 28% of the measured values at the highest pump power.

Although not shown in Fig. 3, a simulation of this experiment was also performed using the 1D code described earlier. For this comparison, a mode area of 230 μm^2 was used that was determined from the eigenmode of a straight fiber. This was the area of an equivalent flat-topped profile with equivalent mode energy. These simulations also matched the data closely, but falling under the measured curve at large pump powers in a similar manner to that of the 3D results. In fact, the 1D and 3D results agree very closely throughout the range of pump powers if the straightened end section is accounted for in the 3D simulations as described above.

IV. Conclusion

We have developed a comprehensive numerical model for the simulation of pulsed fiber amplifiers that includes effects due to both the transverse beam profile and the temporal signature. This model is based on our previous beam propagation approach, and allows for an accurate description of the fiber geometry (with bend loss) using a triangular mesh and an allowance for arbitrary index profiles as before. We include effects due to self-focusing and a two-level gain model that includes gain saturation both in the spatial and temporal domain to allow the simulation of high-power systems. We have begun the benchmarking process by comparisons with simpler 1D simulations as well as direct comparisons with experiment in a power regime high enough to show significant gain saturation, but not other nonlinear effects such as SRS or SBS. Both these exercises have served to satisfactorily validate the accuracy of our model. Future modifications to this model will likely include some predictive capability of the onset of SRS.

V. Acknowledgement

VI. References

1. G. Ronald Hadley, Roger L. Farrow and Arlee V. Smith, Photonics West 2006 paper 6102-63, San Jose, CA 21-26 January, 2006.
2. G. R. Hadley, Int. J. Electron. Commun. **58**, 86 (2004).
3. G. P. Agrawal, "Lateral-mode analysis of gain-guided and index-guided semiconductor-laser arrays", J. App. Phys. 58, 2922(1985).